Development of Computational Tools for 3-D In Vivo Morphometry and Analysis of Deformations of Monkey Optic Nerve Head

Ziyi Zhu[a], Huong Tran[b,c], Andrew P. Voorhees[c], Jacob Wallace[c], Andrew Moore[d], Matthew A. Smith[b,c], Gadi Wollstein[c], and Ian A. Sigal[b,c]

[a] *Department of Mechanical Engineering and Materials Science, Swanson School of Engineering, University of Pittsburgh, Pittsburgh, PA, USA*
[b] *Department of Bioengineering, Swanson School of Engineering, University of Pittsburgh, Pittsburgh, PA, USA*
[c] *Department of Ophthalmology, University of Pittsburgh Medical Center, Pittsburgh, PA, USA*
[d] *Department of Biological Sciences, Kenneth P. Dietrich School of Arts and Sciences, University of Pittsburgh, Pittsburgh, PA, USA*

Abstract

Elevated intraocular pressure (IOP) is the main risk factor for glaucoma, which is characterized by neural tissue loss in the optic nerve head (ONH). The cause of the tissue loss and its relation to IOP is not well understood, although it is widely believed to be, at least in part, due to IOP-related biomechanical insult on the ONH. Our long-term goal is to characterize the deformations of the ONH caused by IOP changes and how these lead to neural tissue loss. This requires precise and robust measurement of ONH morphology. Specifically, in this project we developed Matlab tools to analyze morphology of ONH structures from in vivo optical coherence tomography (OCT) images. Specifically, these tools analyzed the dimensions and positions of 4 important ONH structures: inner limiting membrane (ILM), Bruch membrane (BM), BM opening (BMO), and anterior lamina cribrosa (ALC). From these, ALC, BM and ILM surfaces, the BMO planarity, the minimum rim width (MRW) and the minimum rim area (MRA) were computed. The tools were tested using monkey data acquired under three IOP conditions: normal, low, and high. The ALC depth, BMO planarity, MRW, and MRA under these three IOP conditions were determined. Increase in BMO planarity, as well as decreases in MRA and MRW were observed under high IOP, while the opposite was observed under low IOP. An anterior shift of the ALC depth was also observed under low IOP. Compared to literature values, our measurements of average ALC depth, BMO planarity, MRW, and MRA under normal IOP conditions deviated by 2.3%, 11.4%, 35.8% and 5.9%, respectively, showing consistency with the literature. The program allowed efficient and comprehensive analysis of ONH structures. This, in turn, will facilitate the study of the role of ONH anatomy and biomechanics on susceptibility to glaucoma and of techniques to prevent vision loss.

Keywords: glaucoma, optic nerve head, biomechanics, Matlab

Abbreviations: ONH-Optic Nerve Head, IOP-Intraocular Pressure, ALC-Anterior Lamina Cribrosa, ILM-Inner Limiting Membrane, BM-Bruch Membrane, BMO-Bruch Membrane Opening, OCT-Optical Coherence Tomography, Minimal Rim Width-MRW, Minimal Rim Area-MRA.

1. Introduction

Glaucoma is the second most prevalent cause of blindness worldwide [1]. It is a progressive and irreversible loss of retinal ganglion cell axons, which carry the visual information from the eye to the brain. This axon loss is initiated in the region in the back of the eye called the optic nerve head (ONH), where the retinal ganglion cell axons converge and exit the eye through a collagenous structure called the lamina cribrosa (Figure 1). An elevated intraocular pressure (IOP) of 21 mmHg or higher is considered as a high risk for glaucoma [2], but patients vary in their sensitivities to the elevated IOP. The mechanisms of the neural tissue loss and the origin of the differences in sensitivity to IOP remain unclear, in part because of the challenges in imaging the ONH in vivo and in extracting from these images information on the effects of IOP [3]. These challenges and current efforts to overcome them are discussed in detail in two recent review manuscripts [3], [4]a number of recent advances in optical coherence tomography (OCT. Our group has recently started

imaging rhesus macaque in vivo utilizing optical coherence tomography (OCT), a noninvasive imaging modality that provides real time, 3-D, and high resolution images of the ONH region. We aim to quantify in these images the pressure-induced displacements and deformations of the neural tissue (at the inner limiting membrane-ILM), the Bruch membrane (BM), the scleral canal opening (measured at the Bruch membrane opening-BMO), and the anterior lamina cribrosa (ALC), which are commonly studied structures of the ONH (**Figure 1**) [5]. However, there are a number of challenges in extracting information from the OCT images. First is the ability to compare multiple ONH structures under a given pressure condition or one structure across multiple pressures conditions. Second is the difficulty in acquiring quantitative results to describe these ONH deformations [4]. The purpose of this work was to develop an easy to use set of Matlab tools to resolve these issues and to provide meaningful data of ONH deformation under changing pressures. The program was evaluated by comparing measured outcome parameters from a set of monkey data to the literature.

2. Methods

ONH regions of one monkey eye were imaged in vivo with OCT while controlling for IOP, following methods described elsewhere [6]. Motion artifacts due to breathing and heart rate, identified as a periodic pattern in the known smooth structure of the BM on the slow-scan direction, were removed by translating images in anterior-posterior direction. Manual markings were made on radially resliced images [7] and were reconstructed, using scattered data interpolation, into 3-D surfaces by custom Matlab tools that were previously developed in the laboratory (**Figure 2**). When reconstructing a surface,

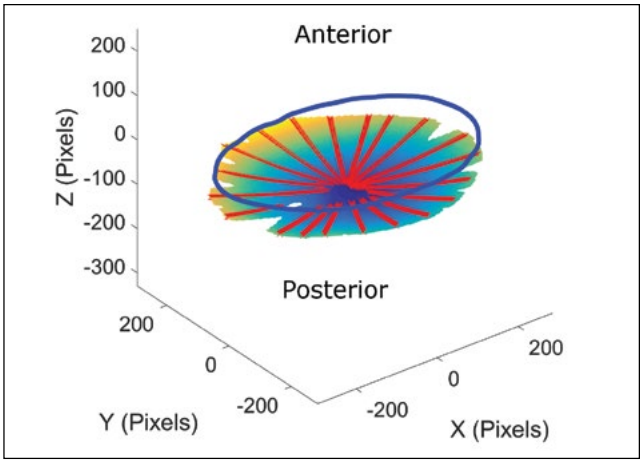

Figure 2: ALC surface reconstructed using the radial markings (red). Blue denotes the outline of the BMO plane used as reference. The surface color represents a heat map of the surface depth.

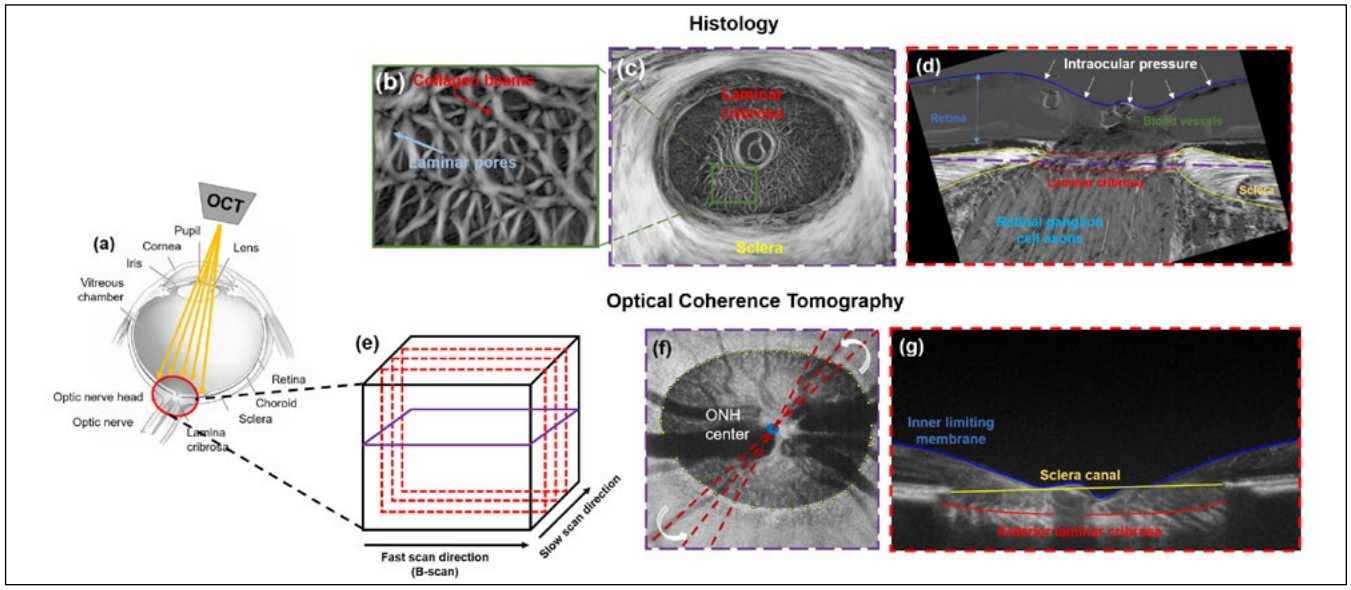

Figure 1: (a) Diagram of the eye, showing the ONH in the back of the eye, which is imaged non-invasively and in 3D with OCT. Top row: (b and c) Coronal sections through the LC shows the microstructures of collagenous beams and pores. (d) An example sagittal histological ONH section. Bottom row: (e) Schematic of a 3D OCT volume of the posterior pole, showing the fast scan direction and the slow scan direction, which may be affected by motion artifacts. (f) Motion artifacts in the slow scan direction are removed, before the volume is resliced radially to obtain virtual radial resliced images for delineations. Shown is a coronal digital section through the OCT volume. (g) Virtual radial resliced image. Colored lines are examples of manual markings

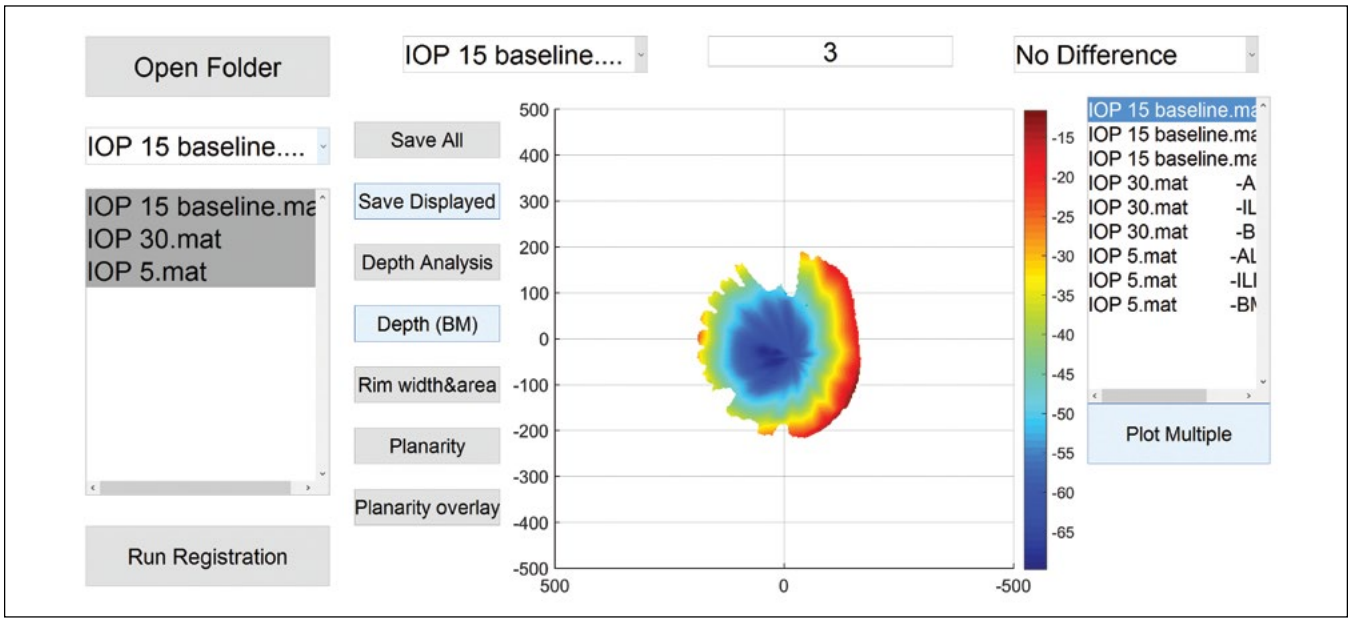

Figure 3: Graphical user interface of the program. Showed in the graphic window was the anterior-posterior view of a ALC surface, colored by the heatmap of the depth.

the program computed a confidence map to determine regions where the interpolated surface was reliable. The program reconstructed and visualized the ALC, BM, and ILM surfaces based on their depth with respect to the best-fit plane of the BMO markings, also known as the BMO plane. The BMO plane was selected because it is a commonly used reference plane in the literature [5], [8], simplifying comparisons. Experimental methods and animal care procedures adhered to the Association for Research in Vision and Ophthalmology (ARVO) Statement for the Use of Animals in Ophthalmic and Vision Research, and were approved by the local Institutional Animal Care and Use Committee (IACUC).

2.1 Surface Depth- ALC, BM, ILM

To analyze the displacement of a surface, the program calculated the mean, median, and standard deviation of its depth. Surfaces across different IOPs were registered using BMO and only differences within overlapping regions were compared as a measure of displacement. However, it is possible that two surfaces with similar mean and median will differ significantly in shape. Thus, to better represent the surface, our program was designed to output the depth distribution curves, using Matlab "histcounts" function, and box plots. The distribution curves provide a general view of how a surface deformed and the box plots simplify discerning quantitatively the amount of displacement. We define the sign of the depth by the relative position with respect to the BMO plane, with anterior to the BMO as positive direction and vice versa. In the surface depth computation, the program used the confidence map to ensure that only reliable regions present in all images were compared to avoid bias. The threshold to define that a region was reliable was determined empirically by identifying the value that maximized surface continuity while avoiding bridging gaps in regions that were not visible.

2.2 BMO Planarity

BMO planarity is a measure of the extent to which the scleral canal, measured at BMO, deviated from a plane. The BMO planarity function applied principal component analysis to the BMO marking to find the best-fit plane and its normal vector, thus allowing calculation of the projection error: the perpendicular distances from the BMO points to the fitted plane. The function generated a plot that visualized the BMOs and the projection, also outputting the normal vector of the plane and the mean of the distances, namely, the BMO planarity. Since several measures are taken with respect to the best-fit BMO plane, it was important to test how well this plane fits the BMO. Small deviations from a plane (small planarities) indicate that the BMO plane is a good representation of the BMO location. Conversely, large deviations (large planarities) suggest that measurements with respect to this plane should be interpreted with caution.

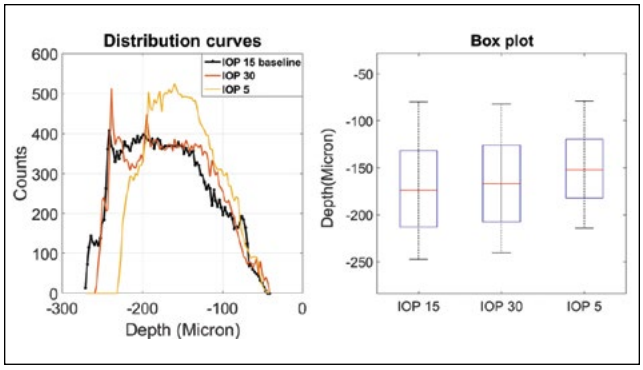

Figure 4: Depth distribution curves (left) and box plot (right) of ALC depth.

2.3 Rim Width and Area

A decrease in the neuroretinal rim tissue thickness has been shown to be an indicator of glaucoma progression [8], and is therefore an important parameter to determine from our images. The 2-D minimum rim width (MRW) segments were first measured in each radial slice as the shortest distance from the BMO to the ILM surface. These were then used to compute the minimum rim area (MRA) by the triangulation of the end points of the MRW segments.

2.4 Application and Evaluation

All the functions were incorporated into a graphical user interface (**Figure 3**) and were tested on a set of monkey eye data from three OCT images under baseline (15 mmHg [9]), low (5 mmHg), and high (30 mmHg) IOP, respectively. The baseline results were compared with the literature data also at baseline.

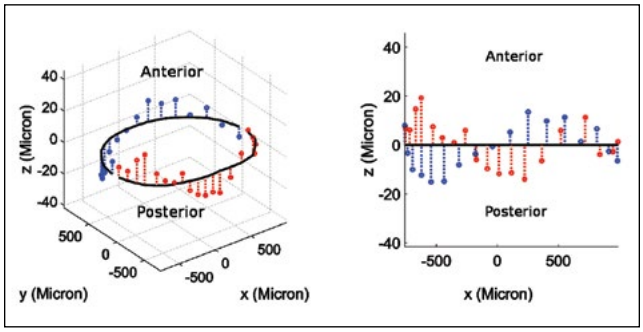

Figure 5: (left) 3D view and (right) side view of the BMO planarity under baseline condition. BMO markings (nasal-temporal side: red-blue dots) were plotted with respect to the outline of the BMO plane (black lines). The z axis was normal to the BMO plane and was stretched 20 times for illustration.

Table 1: ONH parameters of the three test cases and baseline values reported in other studies

Condition	Mean ALC depth (μm)	BMO Planarity (μm)	Minimum rim width (μm)	Minimum rim area (mm^2)
Low IOP (5 mmHg)	-150.0	7.12	195.5	0.987
High IOP (30 mmHg)	-165.8	9.98	187.2	0.938
Baseline (15 mmHg)	-171.0	7.80	192.5	0.941
Baseline in literature	~ -175 [8]	~7 [5]	~300 [8]	1.00±0.19 [10]

3. Results

3.1 ALC Surface Depth

Distribution of the ALC surface depths in the test cases is presented in **Figure 4**. Under 5 mmHg IOP, the ALC depth distribution curve shifted anteriorly, with the median depth decreasing by 12.5% from -174 μm to -152 μm. Under 30 mmHg IOP, the ALC median depth decreased by 4%, from -174 μm to -167 μm. Although the median depth decreased slightly under high IOP, the distribution curve remained close to the baseline case, while under low IOP the curve shifted noticeably as a whole to the anterior.

3.2 BMO Planarity

The BMO planarity is illustrated in **Figure 5** using the case with baseline IOP as an example. The BMOs under three IOP conditions were plotted with respect to the baseline BMO plane in **Figure 6**. BMO planarity was 7.8 μm under baseline condition. Planarity increased by 28% to 9.98 μm at 30 mmHg IOP and decreased by 9.8% to 7.12 μm at 5 mmHg IOP (**Table 1**). Our test

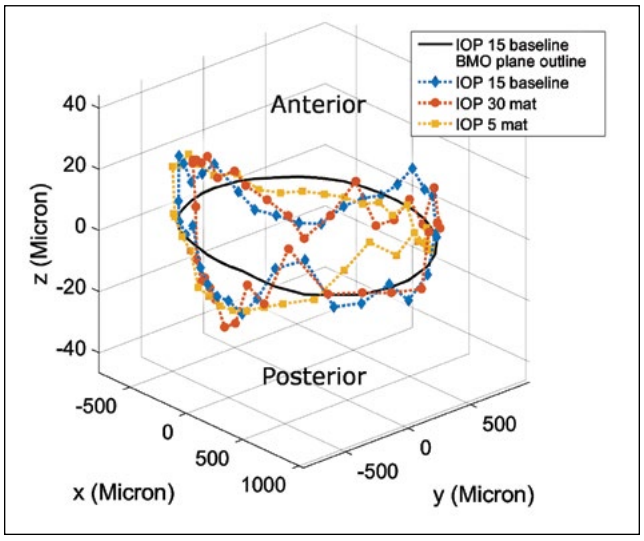

Figure 6: BMO of the three cases. Black is the BMO plane outline under baseline condition. Blue is the baseline, Red is under high IOP, Orange is under low IOP. Note that the Z axis was stretched by 20 times for the purpose of illustration.

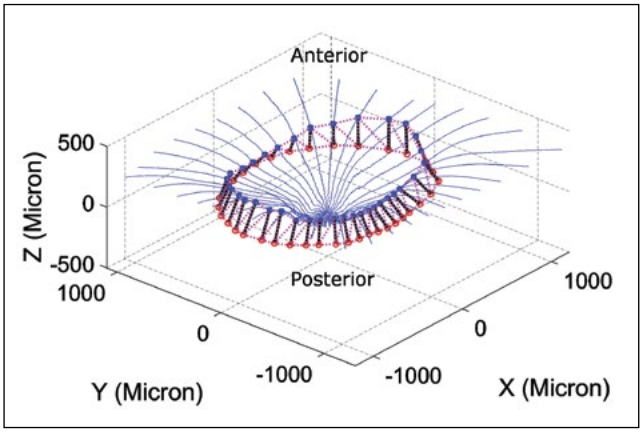

Figure 7: Example minimum rim width and minimum rim area. Figure showing minimum rim width (black) and area (magenta), plotted with BMO markings (red) and ILM surface (blue).

cases showed that increasing IOP led to increased BMO planarity whereas low IOP led to decreased planarity, indicating flattening of the scleral canal opening under low IOP and vice versa.

3.3 Rim Width and Area

Both MRW and MRA (**Figure 7**) decreased with increasing IOP, and increased with decreasing IOP (**Table 1**), reflecting a reduction of the neural tissue thickness under elevated IOP. In this data set, the baseline MRW was 192.5 µm, which decreased by 2.8% to 187.2 µm under high IOP and increased by 1.5% percent to 195.5 µm under low IOP. The MRA was 0.941 mm^2 under the baseline condition, which decreased by 0.3% to 0.938 mm^2 under high IOP and increased by 4.9% to 0.987 mm^2 under low IOP. The percent change in the MRA and MRW were smaller than changes in other ONH measurements.

3.4 Evaluation

All four parameters computed by the program for the three test cases were compared with results from three previous studies in **Table 1** [5], [8], [10]. Compared to the literature, the mean ALC depth, the BMO planarity, the MRW and MRA were 2.3%, 11.4%, 35.8% and 5.9% different, respectively. Although, the MRW computed in the test case showed a 35.8% deviation from the previous study, all other results were comparable with literature, showing less than 15% deviation.

4. Discussion

Our program allows 3-D quantitative analysis of in vivo OCT images of the monkey ONH. The user-friendly design enables the extraction of important biomechanical information from in vivo images efficiently through an integrated interface, with several useful functions requiring no more than a single click. The program was tested with a set of experimental data obtained under three IOP conditions.

The ALC depth distribution curve reflected the anterior shift of the ALC surface under low IOP. Also, our results indicated that the BMO planarity increased under high IOP and decreased under low IOP, suggesting a deformation of the scleral canal under elevated IOP. The change in the MRW and MRA were relatively small, however both measures increased from baseline under low IOP and decreased with high IOP, indicating that thickness of the neuroretinal rim tissue increases as IOP decreases, and vice versa

Compared with previous studies, we observed a deviation under 15% for the ALC depth, BMO planarity and MRA. We did find a deviation of 35.8% from literature values for the MRW. The reference literature value for the BMO planarity was obtained from human subjects, whereas all the other measurements were obtained from monkeys. This might contribute to explain the difference in BMO planarity, although human and monkey are often regarded to have similar ONH structures and biomechanics [11]. Also, our images were acquired while the animals were under controlled intracranial pressure. The literature with which we compared values provided no information on intracranial pressure. Several recent studies, including some from our group, have demonstrated that variations in intracranial pressure can affect the ONH [6], [12].

While being a powerful computational tool, our Matlab program still has room for improvements. First, while this work presented comparison between our results and literatures, more rigorous validation will be included in future work. Also, we would like to improve robustness to incomplete data, such as when the structures cannot be discerned because of OCT signal shadowing behind blood vessels. Furthermore, future work will involve adding new functionalities to the program, such as analyzing the regional depth and computing shape indexes of the surfaces, allowing the extraction of more valuable information from the OCT images.

5. Conclusion

Our work has produced a set of tools integrated into a Matlab program. The tools compute and visualize several parameters, namely the ALC, BM, ILM surface depth, the BMO planarity, the MRW and MRA, which are important for characterizing the morphology and mechanics of the ONH structures in response to IOP changes. The analyses can be executed easily with a single click on the graphical user interface. The program developed in this work was tested with a set of in vivo monkey data, and showed results comparable to the literature. It is ready to be employed in research of the ONH biomechanics and has the potential to be applied to other studies that require similar 3-D surface data analysis.

6. Acknowledgments

The project was funded jointly by the National Institutes of Health (R01 EY023966, EY025011, EY013178, T32 EY017271 and P30 EY008098), Glaucoma Research Foundation Shaffer Grant, the Swanson School of Engineering, and the Office of the Provost.

7. References

[1] I. C. Campbell, B. Coudrillier, and C. R. Ethier, "Biomechanics of the posterior eye: A critical role in health and disease.," *J. Biomech. Eng.*, vol. 136, no. February, Dec. 2013.

[2] A. Sommer, M. JTielsch, and J. Katz, "Relationship between intraocular pressure and primary open angle glaucoma among white and black americans: The baltimore eye survey," *Arch. Ophthalmol.*, vol. 109, no. 8, pp. 1090–1095, Aug. 1991.

[3] I. A. Sigal, B. Wang, N. G. Strouthidis, T. Akagi, and M. J. A. Girard, "Recent advances in OCT imaging of the lamina cribrosa.," *Br. J. Ophthalmol.*, vol. 98 Suppl 2, no. Suppl 2, p. ii34-9, Jul. 2014.

[4] M. J. a Girard, W. J. Dupps, M. Baskaran, G. Scarcelli, S. H. Yun, H. a Quigley, I. a Sigal, and N. G. Strouthidis, "Translating Ocular Biomechanics into Clinical Practice: Current State and Future Prospects.," *Curr. Eye Res.*, vol. 40, no. April, pp. 1–18, 2014.

[5] S. Lee, S. X. Han, M. Young, M. F. Beg, M. V. Sarunic, and P. J. Mackenzie, "Optic Nerve Head and Peripapillary Morphometrics in Myopic Glaucoma," *Investig. Opthalmology Vis. Sci.*, vol. 55, no. 7, p. 4378, Jul. 2014.

[6] H. Tran, A. P. Voorhees, B. Wang, N.-J. Jan, E. Tyler-Kabara, L. Kagemann, H. Ishikawa, J. S. Schuman, M. A. Smith, G. Wollstein, and I. A. Sigal, "In vivo Modulation of Intraocular and Intracranial Pressures Causes Nonlinear and Non-monotonic Deformations of The Lamina Cribrosa," *Assoc. Res. Vis. Ophthalmol.*, 2016.

[7] W. Jacob, H. Tran, T. Jeremy, A. Voorhees, J. Ten Eyck, D. Tsui, J. R. Drobitch, Y. Shi, W. Walters, B. Wang, M. A. Smith, E. Tyler-Kabara, J. S. Schuman, G. Wollstein, and I. A. Sigal, "Improving 3D Quantification of In-Vivo Monkey Optic Nerve Head Deformations Using Radial Methods on Optical Coherence Tomography Images," *Univ. Pittsburgh-Science 2015*, 2015.

[8] N. G. Strouthidis, B. Fortune, H. Yang, I. a Sigal, and C. F. Burgoyne, "Longitudinal change detected by spectral domain optical coherence tomography in the optic nerve head and peripapillary retina in experimental glaucoma.," *Invest. Ophthalmol. Vis. Sci.*, vol. 52, no. 3, pp. 1206–19, Mar. 2011.

[9] Y. Suzuki, A. Iwase, M. Araie, T. Yamamoto, H. Abe, S. Shirato, Y. Kuwayama, H. K. Mishima, H. Shimizu, G. Tomita, Y. Inoue, and Y. Kitazawa, "Risk Factors for Open-Angle Glaucoma in a Japanese Population: The Tajimi Study," *Ophthalmology*, vol. 113, no. 9, pp. 1613–1617, 2006.

[10] B. Fortune, J. Reynaud, C. Hardin, L. Wang, I. A. Sigal, and C. F. Burgoyne, "Experimental Glaucoma Causes Optic Nerve Head Neural Rim Tissue Compression: A Potentially Important Mechanism of Axon Injury," *Investig. Opthalmology Vis. Sci.*, vol. 57, no. 10, p. 4403, Aug. 2016.

[11] H. Levkovitch-Verbin, "Animal models of optic nerve diseases," *Eye*, vol. 18, no. 11, pp. 1066–1074, Nov. 2004.

[12] W. H. Morgan, B. C. Chauhan, D.-Y. Yu, S. J. Cringle, V. a Alder, and P. H. House, "Optic disc movement with variations in intraocular and cerebrospinal fluid pressure.," *Invest. Ophthalmol. Vis. Sci.*, vol. 43, no. 10, pp. 3236–42, Oct. 2002.